Fully coupled six-dimensional calculations of the water dimer vibration-rotation-tunneling states with split Wigner pseudospectral approach. II. Improvements and tests of additional potentials

R. S. Fellers, L. B. Braly, and R. J. Saykally[a)]
Department of Chemistry, University of California, Berkeley, California 94720-1460

C. Leforestier
Laboratoire Structure et Dynamique des Systèmes Moléculaires et Solides (UMR 5636), CC 014, Université des Sciences et Techniques du Languedoc, 34095 Montpellier Cédex 05, France

(Received 14 September 1998; accepted 29 December 1998)

The SWPS method is improved by the addition of H.E.G. contractions for generating a more compact basis. An error in the definition of the internal fragment axis system used in our previous calculation is described and corrected. Fully coupled 6D (rigid monomers) VRT states are computed for several new water dimer potential surfaces and compared with experiment and our earlier SWPS results. This work sets the stage for refinement of such potential surfaces via regression analysis of VRT spectroscopic data. © *1999 American Institute of Physics.* [S0021-9606(99)00413-4]

I. INTRODUCTION

While intermolecular forces have been studied for many years, the field has progressed most rapidly in the past decade due to advances in both experiment and theory. On the experimental front, microwave and terahertz molecular beam spectrometers have provided detailed high resolution spectra of a large number of weakly bounded clusters. The spectra from these methods serve as an exacting probe of the intermolecular potential energy surface (IPS), which are the ultimate products of such investigations. Of particular importance are the recent terahertz vibration-rotation-tunneling (VRT) spectra of water clusters[1–12] which provide a new route for formulating model potentials which can describe the interesting and complex behavior of bulk water. Simultaneously, a large number of IPS's have been computed at various levels of *ab initio* theory; a significant number of these are water pair potentials. The predictive power of such potentials is examined by testing their ability to mimic the properties of bulk water in molecular dynamics simulations, and the equilibrium structures of small water clusters, and the structure of bulk ice. However, recent advances in computational methods and the ever increasing accessibility of high performance computers have made it possible to calculate actual spectroscopic observables from these IPS and for direct comparison with experiment. Given this capability, one would ultimately seek to determine a globally accurate IPS, viz., those able to replicate bulk properties and spectra with quantitative accuracy.

Experimental IPS determinations have proceeded via least squares fits of microwave and IR VRT spectra with constraints from other available data (multipole moments, dispersion coefficients, virial coefficients, polarizabilities, etc.). The most effective methods for calculating the eigenstates of a multidimensional IPS are the variational method with an $\mathcal{L}^2$ finite basis representation (FBR) and grid methods such as collocation or the discrete variable representation (DVR).

With all FBR approaches it is generally found that at least 10 basis functions per degree of freedom are required for spectroscopic accuracy. For the case of two rigid linear molecules (a 4D system) this entails solving an eigenvalue problem of $O(N=10^4)$. Elrod and Saykally used the FBR method to determine the 4D IPS of $(HCl)_2$ with rigid monomers.[13] This method scales unpropitiously, however, as Elrod and Saykally found solving the 6D IPS (flexible monomers) to be prohibitive on the basis of CPU time ($O(N^3)$) and memory requirements ($O(N^2)$). Nevertheless, in an impressive piece of work, Otholf *et al.* used the FBR method to determine a 6D IPS for $(NH_3)_2$ by a trial and error comparison with measured properties of the dimer (microwave and terahertz VRT spectra, dipole moments, and nuclear quadrupole splittings).[14,15] The expense of the calculation precluded a rigorous IPS determination via regression analysis, however.

Grid methods, wherein the basis functions are transformed into a set of amplitudes associated with a discrete set of points in coordinate space, dramatically simplify the evaluation of matrix elements of coordinate operators, such as the potential energy. Collocation[16] was employed to determine the 3D (rigid monomers) IPS for $Ar\cdot H_2O$ (Refs. 17, 18) and $Ar\cdot NH_3$.[19] The collocation method engenders a very simple computer code and complete generality with respect to the form of the potential and basis functions but suffers from the instability and inefficiency associated with the nonsymmetric dense eigenvalue problem. The discrete variable representation of Light and co-workers[20] improves over collocation by producing eigenvalue problems that are both symmetric and sparse. These features are particularly important because this class of problem is amenable to iterative eigensolvers such as Lanczos[21] or Arnoldi[22] which have linear scaling both in terms of execution time and storage re-

a)Author to whom correspondence should be addressed.

quirements. In an IPS determination for Ar·OH, Hayes and co-workers demonstrated a 100-fold increase in speed by using DVR vs collocation.[23] Bačić and co-workers have recently obtained the VRT states of $(HCl)_2$ in a fully coupled 6D DVR calculation with a flexible monomer IPS.[24,25] Such formulations of the DVR require the use of direct product basis functions which become extremely large for high dimensional systems.

Prior to the introduction of DVR, Feit and Fleck,[26,27] and Kosloff and Kosloff[28,29] initiated the split Hamiltonian formulation. This method exploits two different representations associated with the Hamiltonian operator. In its original formulation, the kinetic energy was evaluated in the spectral representation (plane waves), while a grid was used for the potential. These two representations are equivalent, being related by a unitary transformation. Later, Friesner *et al.* used a split representation in a bound state calculation termed the adiabatic pseudospectral (APS) method.[30]

The split Hamiltonian method has been applied by one of us (C.L.) for the computation of the VRT states of $Ar·H_2O$.[31] An important advancement presented in that work was the definition of a grid associated with a basis of (nondirect product) Wigner functions which form a very efficient basis for such problems. Moreover, the calculation maintained the variational principle by using a grid size significantly larger than the spectral representation dimension. This method is referred to as the split Wigner pseudospectral (SWPS) method.

In subsequent work, Leforestier *et al.* extended the SWPS to the fully coupled 6D water dimer problem wherein they demonstrated the efficiency of the approach by determining the VRT states of four well known water potentials.[32] Unfortunately, an error in the SWPS computer code invalidated the actual VRT states calculated in that work. In this paper we describe further improvements in the SWPS method and the error in the previous implementation. The outline of the paper is as follows. In Sec. II, we describe the feasible tunneling motions of the water dimer and how they are manifested in the microwave and VRT spectra. In Sec. III, we restate the SWPS method and the improvements applied to the water dimer and clearly point out the error in the previous implementation. Section IV investigates the convergence properties of SWPS. In Sec. V, we present the calculated VRT states of several potentials, both correcting the results of the previous paper and testing additional potentials. Section VI presents our conclusions.

II. WATER DIMER DATA

There are a maximum of 16 equivalent structures of the water dimer that can be generated without breaking any covalent bonds. The hydrogen bonding in the dimer rearranges by quantum tunneling along low-energy barrier pathways on the IPS to access the different structures. Permutation of the nuclei gives rise to 8 equivalent structures or versions in the nomenclature of Bone *et al.*[33] Inversion of these structures through the center of mass generates 8 additional configurations. If the equilibrium structure contains a plane of symmetry, as the evidence currently supports, then there are only

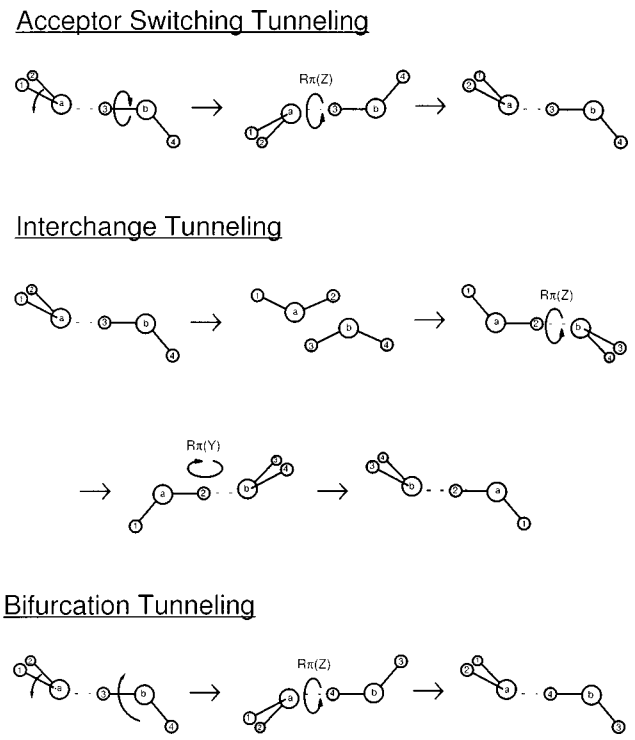

FIG. 1. The proposed lowest energy pathways for hydrogen bond rearrangement.

8 distinct versions. The permutation inversion (PI) symmetry group G_{16} is typically used to explain the resulting splittings in the rovibrational levels. G_{16} is isomorphic with the $D_{4h}(M)$ point group and is consistent with observed VRT dynamics.[34]

The motion that we term ''acceptor switching'' has the lowest energy barrier making it the most facile tunneling motion on the IPS. This motion allows for the exchange of the protons in the water molecule acting as the H-bond acceptor. Figure 1 shows the proposed rearrangement pathway, but the net effect is a C_2 rotation of the acceptor about its symmetry axis. Each rovibrational energy level of the semirigid water dimer is split into two as shown in Fig. 2 as a result of this rearrangement.

The next most feasible tunneling motion is identified as ''interchange.'' There are several possible pathways, with the most likely being the geared rotation shown in Fig. 1. In interchange tunneling, the roles of the individual donor and acceptor water molecules are reversed. The effect is to further split each of the energy levels into three, but to a much smaller degree than that of acceptor tunneling. These two tunneling motions resolve all degeneracies in the water dimer, inducing a sixfold splitting in parity nondegenerate states.

The final rearrangement identified is ''donor,'' or ''bifurcation'' tunneling, wherein the H-bond donor permutes its protons. The barrier to this motion is relatively high and produces a small shift of the VRT levels, but causes no further splitting.

The water dimer has been the subject of a large number of theoretical and experimental studies. High resolution microwave,[35–45] terahertz,[1,2] and mid-IR (Refs. 12, 46) spec-

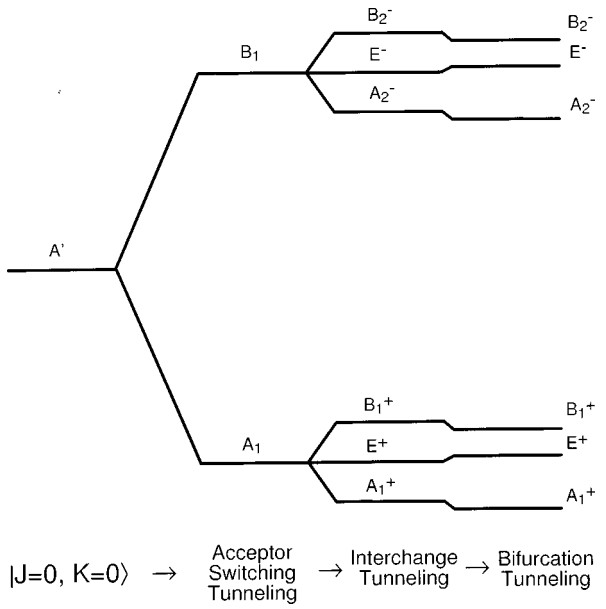

FIG. 2. The experimental splittings.

tra have all been measured. From these investigations, the hydrogen bond tunneling dynamics occurring in low K levels of the ground state and the first excited acceptor bending state are well characterized,[1,2] and several other intermolecular vibrations have recently been measured and partially analyzed.[47] Several different dynamical methods have recently been employed to calculate the VRT states corresponding to a variety of IPS that have been determined for this system. Lewerenz and Watts[48] have used QMC to calculate the tunneling splittings and intermolecular vibrations of the RWK2 surface, while Gregory and Clary[49] used a DQMC method to calculate the ground state structure of the RWK2 and ASP surfaces. Althorpe and Clary[50] employed the reversed adiabatic approximation (RAA) to calculate the ground state tunneling splittings and several intermolecular vibrations, again using RWK2 and ASP in a 5D approximation to the coupled dynamics. A number of ab initio calculations have addressed this system (see Ref. 51, and references therein), generally calculating the minimum energy structures with harmonic frequencies and intensities,[52–54] but other studies have also investigated tunneling barriers and possible tunneling paths connecting the equivalent minima.[55,56]

III. METHOD OF CALCULATIONS

Although the split Wigner pseudo spectral method has been described in complete detail,[32] the method is summarized here to provide a context for explanation of the improvements made since the previous publications. For the Hamiltonian, we use the Brocks *et al.*[57] body fixed rigid rotor formulation

$$\mathbf{H}=-\frac{\hbar^2}{2\mu_{AB}}\frac{\partial^2}{\partial R^2}+\mathbf{H}_{\mathrm{rot}}^{(A)}+\mathbf{H}_{\mathrm{rot}}^{(B)}+\mathbf{V}(R,\mathbf{\Omega}^{(A)},\mathbf{\Omega}^{(B)})+\frac{1}{2\mu_{AB}R^2}\{\mathbf{J}^2+\mathbf{j}^2-2\mathbf{j}\cdot\mathbf{J}\}, \quad (1)$$

TABLE I. Water dimer parameters used in the calculations.

$R_{\mathrm{O-H}}=1.808\,846$ a.u.	$\angle\mathrm{HOH}=104.52°$	$\mu_{\mathrm{H_2O,H_2O}}=9.005\,25$ amu
$B_x=9.2778\ \mathrm{cm}^{-1}$	$B_y=27.8806\ \mathrm{cm}^{-1}$	$B_z=14.5216\ \mathrm{cm}^{-1}$

where

(1) R is the distance between the centers of mass of the two monomers A and B, and μ_{AB} their reduced mass,
(2) $\mathbf{H}_{\mathrm{rot}}^{(\alpha)}$ and $\mathbf{j}_\alpha$ are, respectively, the rotational Hamiltonian and angular momentum of the monomer α,
(3) $\mathbf{j}=\mathbf{j}_A+\mathbf{j}_B$ is the coupled internal rotational angular momentum,
(4) $\mathbf{J}=\mathbf{j}+l$ the total angular momentum (l is the angular momentum of the monomer centers of mass),
(5) and $\mathbf{\Omega}^{(\alpha)}\equiv(\varphi^{(\alpha)},\theta^{(\alpha)},\chi^{(\alpha)})$ represents the Euler angles defining the orientation of monomer α in the body fixed axes.

The parameters used in the calculations are given in Table I. The source of the error in the previous paper was in the definition of internal rotational axis on each monomer. In the former work, we had mistakenly used the type **Ir** representation on the monomers' rotational constants whereas the symmetrized basis formulation, given in Table II, had been derived for **IIr**. Here we reorder the monomer axis to **IIr** in order to be consistent with the symmetrized basis.

The spectral representation of the basis is written as a direct product of

$$\mathcal{B}_{\mathrm{ang}}\otimes\{|S_n\rangle,n=1,N_s\}, \quad (2)$$

where the $|S\rangle$ are sine functions. $\mathcal{B}_{\mathrm{ang}}$ is either an uncoupled direct product of Wigner functions for each monomer and the overall dimer

$$\mathcal{B}_{\mathrm{unc}}=\{|j_A,k_A,\omega_A\rangle\otimes|j_B,k_B,\omega_B\rangle\otimes|J,\Omega,M\rangle\} \quad (3)$$

TABLE II. Symmetry adapted linear combination vectors for the different irreducible representations Γ. λ is defined as $J+j_A+j_B$. This basis assumes a type **IIr** representation of the water monomers. An example of the symmetrization scheme can be found in the work of van Bladel *et al.* (Ref. 80).

$\lvert\xi_1,\Omega\rangle$	$\lvert j_A j_B k_A k_B;j\Omega\rangle$	
$\lvert\xi_2,\Omega\rangle$	$\lvert j_A j_B k_A k_B;j\overline{\Omega}\rangle$	
$\lvert\xi_3,\Omega\rangle$	$\lvert j_A j_B \overline{k_A k_B};j\overline{\Omega}\rangle$	
$\lvert\xi_4,\Omega\rangle$	$\lvert j_A j_B \overline{k_A k_B};j\Omega\rangle$	
Γ	$\lvert j_A j_B k_A k_B;j\Omega,\Gamma\rangle$	(k_A,k_B) parity
A_1^+	$\xi_1+(-1)^\lambda\xi_2+(-1)^{\lambda+j}\xi_3+(-1)^j\xi_4$	*ee*
A_2^+	$\xi_1-(-1)^\lambda\xi_2+(-1)^{\lambda+j}\xi_3-(-1)^j\xi_4$	*oe*
B_1^+	$\xi_1-(-1)^\lambda\xi_2+(-1)^{\lambda+j}\xi_3-(-1)^j\xi_4$	*ee*
B_2^+	$\xi_1+(-1)^\lambda\xi_2+(-1)^{\lambda+j}\xi_3+(-1)^j\xi_4$	*oo*
E^+	$\xi_1+(-1)^{\lambda+j}\xi_3$	*oe* or *eo*
	$\xi_2+(-1)^{\lambda+j}\xi_4$	*oe* or *eo*
A_1^-	$\xi_1+(-1)^\lambda\xi_2-(-1)^{\lambda+j}\xi_3-(-1)^j\xi_4$	*ee*
A_2^-	$\xi_1-(-1)^\lambda\xi_2-(-1)^{\lambda+j}\xi_3+(-1)^j\xi_4$	*oe*
B_1^-	$\xi_1-(-1)^\lambda\xi_2-(-1)^{\lambda+j}\xi_3+(-1)^j\xi_4$	*ee*
B_2^-	$\xi_1+(-1)^\lambda\xi_2-(-1)^{\lambda+j}\xi_3-(-1)^j\xi_4$	*oo*
E^-	$\xi_1-(-1)^{\lambda+j}\xi_3$	*oe* or *eo*
	$\xi_2-(-1)^{\lambda+j}\xi_4$	*oe* or *eo*

TABLE III. A demonstration of the convergence of the eigenenergies for the $J=0$ ground state symmetries as a function of the size of the monomer angular basis set. The above results are from a series of 5D calculations of the ASP-W potential; the radial coordinate was fixed at 5.62 a.u. Energies are in cm^{-1}.

Monomer basis size $j_{max}=k_{max}=\omega_{max}$	7	8	9	10	11	12
A_1^+	−1052.097	−1054.178	−1054.786	−1054.942	−1054.985	−1055.010
B_1^+	−1048.083	−1050.403	−1051.063	−1051.239	−1051.289	−1051.312
A_2^-	−1048.653	−1050.761	−1051.428	−1051.577	−1051.620	−1051.644
B_2^-	−1044.803	−1047.133	−1047.857	−1048.023	−1048.072	−1048.095
E^+	−1049.784	−1051.974	−1052.666	−1052.832	−1052.873	−1052.896
E^-	−1046.744	−1048.843	−1049.553	−1049.722	−1049.767	−1049.789

or a coupled representation

$$\mathcal{B}_{cpl}=\{|j_A j_B k_A k_B ; j\Omega\rangle|J,\Omega,M\rangle\}. \tag{4}$$

From the coupled basis, we use the G_{16} permutation-inversion symmetry group of the water dimer to symmetrize the basis into the 10 available irreducible representations (Ireps) Γ's. The symmetry adapted vectors are constructed as

$$\begin{aligned}|j_A j_B k_A k_B ; j\Omega\Gamma\rangle &= c_1^{(\Gamma)}|j_A j_B k_A k_B ; j\Omega\rangle + c_2^{(\Gamma)}|j_B j_A k_B k_A ; j\Omega\rangle \\ &\quad + c_3^{(\Gamma)}|j_A j_B \bar{k}_A \bar{k}_B ; j\bar{\Omega}\rangle + c_4^{(\Gamma)}|j_B j_A \bar{k}_B \bar{k}_A ; j\Omega\rangle,\end{aligned} \tag{5}$$

where $\bar{k}\equiv -k,\Gamma$ is the symmetry label, and the c_i are given in Table II.

The kinetic energy terms are evaluated in the coupled-spectral basis, where the terms are analytic, and the potential is evaluated on a grid of six-coordinates (five Euler angles and one radial coordinate, $\{\theta^{(A)},\chi^{(A)},\theta^{(B)},\chi^{(B)}, \varphi=\varphi^{(A)-(B)},R\}$). Transformation of the spectral basis onto the grid and back is accomplished via a series of collocation matricies and FFT's. Explicit details of this procedure are found in our previous publications.[31,32]

In the original version of the SWP code, the radial part of the wave functions were described by uncontracted sine functions $\{|S_n\rangle,n=1,N_p\}$. Transformation of the sines on to the grid of radial points $\{R_p=R_{min}+p\Delta R\}$ is accomplished by a collocation matrix

$$U_{pn}^{(R)}=\sqrt{\frac{2}{N_R+1}}\sin\frac{n\pi p}{N_R+1}. \tag{6}$$

In the usual case, the number of radial points is N_p+3, where N_p is the highest order in the sine basis and is typically in the range of 10–13.

To reduce the required number of DVR points along the radial coordinate necessary to achieve convergence of the eigenenergies, we contract the elementary sine basis set and use a variation[58] of the H.E.G. scheme[59,60] to select an optimal set of radial points. The method is as follows.

The full 6D potential is sampled to determine a suitable 1D cut of the potential along the radial coordinate. This is done by sampling the potential at a set of N_p+3 evenly space points along R and varying the angular degrees of freedom until the minimum is found at each point R. This 1D potential is referred to as $V_{eff}(p)$. With this potential, we form a 1D Hamiltonian,

$$\mathbf{H}=-\frac{\hbar^2}{2\mu_{AB}}\frac{\partial^2}{\partial R^2}+V_{eff}(p) \tag{7}$$

and follow the potential optimized DVR (PO-DVR, a multi-dimension H.E.G. scheme) procedure of Echave and Clary.[58] In practice, when sampling the potential to form the 1D Hamiltonian, $N_p\approx 13$ to afford a reasonably accurate picture of the potential and to have enough sine basis functions for a nearly complete contracted basis. Once the new basis functions and optimized points are found, only a subset of the points and functions associated with the lowest 1D eigenenergies are retained for the 6D calculation. The minimum size of this subset is determined experimentally.

IV. COMPUTATIONAL ASPECTS

In the previous paper, we reported results from convergence tests with respect to the size of angular basis. In that discussion we found that for the four potentials previously investigated, to achieve a convergence of the relative energies to at least 0.01 cm^{-1}, it was necessary to have $j_{max}\geqslant 10$. Also shown were the general effects on the tunneling

TABLE IV. The convergence of the tunneling splittings and shifts for the $J=0$ ground state as a function of monomer basis set size. These data were derived from Table III.

Monomer basis size $j_{max}=k_{max}=\omega_{max}$	7	8	9	10	11	12
Acceptor splitting	3.444	3.417	3.358	3.365	3.365	3.366
Lower interchange splitting	4.014	3.775	3.723	3.703	3.696	3.698
Upper interchange splitting	3.850	3.628	3.571	3.554	3.548	3.549
Lower bifurcation shift	2.313	2.204	2.120	2.110	2.112	2.114
Upper bifurcation shift	1.909	1.918	1.875	1.855	1.853	1.855

TABLE V. The convergence of the tunneling splittings and shifts for the $J=0$ ground state with a restricted angular basis with $|\omega_{max}|=|k_{max}|\leqslant j_{max}=12$. All other conditions are as presented in Table III.

Monomer basis size $\|\omega_{max}\|=\|k_{max}\|$	7	8	9	10	11	12
Acceptor splitting	3.056	3.435	3.355	3.367	3.365	3.366
Lower interchange splitting	3.755	3.703	3.698	3.700	3.697	3.698
Upper interchange splitting	3.551	3.564	3.548	3.552	3.549	3.549
Lower bifurcation shift	1.977	2.152	2.108	2.116	2.113	2.114
Upper bifurcation shift	2.045	1.825	1.860	1.855	1.855	1.855

splittings if we allowed $|k_{max}=\omega_{max}|<j_{max}$. What was not shown, however, was the rate of convergence with respect to the size of the angular basis, which has been added below. Also added are data concerning the convergence of the energies with respect to the radial basis.

A. Angular basis

In the description of the monomer basis functions, $|j_\alpha,k_\alpha,\omega_\alpha\rangle$, the allowed ranges of the monomer quantum numbers are $|\omega_\alpha|\leqslant j_\alpha$, $|k_\alpha|\leqslant j_\alpha$, and $0\leqslant j_\alpha\leqslant j_{max}$. The convergence tests consist of increasing j_{max}. In all cases, we have constrained $\omega_{max}=k_{max}=j_{max}$. The number of quadrature points was set so that for the θ grid, $N_\theta=j_{max}+3$ and for the χ and φ grids, $N_\chi=N_\varphi\geqslant(2j_{max}+1)+2$. The inequality reflects the fact that the χ and φ grids are handled by FFT's which have a restriction on the allowed dimensions (requiring dimensions that are powers of 2, 3, or 5).

In the tests shown below, we have calculated the eigenstates of $J=0$ ground state manifold using the ASP-W potential[61] in a series of 5D runs. In all cases, R was fixed at 5.62 a.u., near the equilibrium geometry, and the constraint of $\omega_{max}=k_{max}=j_{max}$ was used. The results are presented in Tables III and IV.

In Table III are the absolute energies of the six lowest eigenstates. The trends to note are that in increasing j_{max} from 7 to 12, all the energies have decreased by about 3 cm^{-1}, and with increasing j_{max} from 11 to 12, the energies have converged to $\approx\pm0.025$ cm^{-1}.

When considering the relative energies, as shown in Table IV, the convergence is much faster. By increasing j_{max} from 7 to 12, the tunneling splittings in the $J=0$ manifold have only decreased by 0.3 cm^{-1} or less, and by $j_{max}=12$ we find that the deviation is on the order of ±0.001 cm^{-1}. We note that by $j_{max}=9$, the relatives energies have converged to within $\approx\pm0.02$ cm^{-1} of the final values. This is important in regards to computability as the increase of j_{max} from 9 to 12 represents more than a fourfold increase in memory requirements and floating point operations.[62]

B. Restricted angular basis

To further test the angular convergence, we relaxed the k and ω constraint so that $|\omega_{max}|=|k_{max}|\leqslant j_{max}$. In a series of 5D calculations, we set $j_{max}=12$ and simultaneously varied k and ω over a range of 7–12. The results for the $J=0$ splittings are presented in Table V. These data show that we can reduce ω_{max} and k_{max} to as much as $j_{max}-3$ with little reduction in the accuracy of the calculated splittings.

C. Radial basis

To test the utility of using the H.E.G. contraction in the SWP code, we performed a number of calculations both with and without the contraction to ascertain the effects on both the tunneling splitting and shifts and the absolute energies of the eigenstates. In the following examples, the ASP-W potential was used along with an angular basis set ($j_{max}=k_{max}=\omega_{max}$) large enough to converge the $J=0$ tunneling splittings to better than 0.01 cm^{-1} (absolute energies are converged to ~0.05 cm^{-1}). For all the calculations the sampling range of the radial points (c.m. to c.m. of the water monomers) was 4.3–9.0 a.u.

To quantify the effectiveness of the contraction, we report the five calculated splittings and shifts in the $J=0$ VRT states as well as the absolute energy of the $J=0$ A_1^+ state, or D_0 (the dissociation energy).

In the results of Table VI, we show the $J=0$ states determined without using the HEG contraction. In reducing the number of radial points from 16 to 7, there is an increase of more than 3 cm^{-1} in the acceptor tunneling splitting representing a nearly 70% change. Both interchange splittings vary by more than 1 cm^{-1}, or around 30%.

In contrast, the effects of the H.E.G. contraction as shown in Table VII, show a marked improvement. When the number of retained H.E.G. radial points is reduced from 13 to 4, the acceptor tunneling splitting is reduced by 0.104 cm^{-1}, or less than 3%. The lower interchange splitting is increased by 0.035 cm^{-1}, a 1% change. The effect on the upper interchange splitting is smaller still. Likewise, we see a similar effect on the donor shifts. We note that if the number of radial points is reduced further to 3, there is a significant increase in the errors. The most likely cause is probably due to the fact that with 3 points, only 1 radial function is available to solve the 6D Hamiltonian.

TABLE VI. Tunneling splittings and shifts without H.E.G. contraction. The sampling range of the potential is 4.3–9.0 a.u. Energies are given in wave numbers.

Radial points	16	13	10	7
Acceptor splitting	4.686	4.717	5.382	7.872
Lower interchange splitting	3.469	3.603	3.689	2.285
Upper interchange splitting	3.483	3.624	3.784	2.395
Lower bifurcation shift	2.131	2.201	2.321	1.981
Upper bifurcation shift	1.904	1.971	2.096	1.699
D_0	986.245	984.082	968.069	909.376

TABLE VII. Tunneling splitting and shifts calculated with H.E.G. contraction scheme. The sampling range of the potential is 4.3–9.0 a.u. Energies are given in wave numbers.

Radial points	13	10	8	6	4	3
Acceptor splitting	4.670	4.664	4.669	4.682	4.566	3.158
Lower interchange splitting	3.439	3.440	3.441	3.450	3.474	5.499
Upper interchange splitting	3.449	3.449	3.451	3.461	3.458	5.212
Lower bifurcation shift	2.114	2.115	2.115	2.121	2.122	2.943
Upper bifurcation shift	1.887	1.887	1.888	1.894	1.887	2.584
D_0	986.584	986.611	986.574	986.418	986.037	986.002

V. RESULTS

A. Assessing model potentials: ASP, MCY, NEMO, SW

To identify potentials that can best describe the VRT spectra of the water dimer, we have calculated the low energy eigenstates of a number of water pair potentials. The results presented here are the two original ASP potentials of Millot and Stone (which we term ASP-W and ASP-S),[61] the MCY potential of Matsuoka, Clementi, and Yoshimine,[63] the NEMO potential of Karlström *et al.*,[64] a potential due to Kuwajima and Warshel (here after referred to as MCY-KW),[65] and the SW potential due to Wheatley.[66] For all the potentials investigated, we employed fully coupled 6D calculations over the range of $R=4.3$–9.0 a.u. with $j_{\max}=k_{\max}=\omega_{\max}=10$. We did not extend the angular basis further as increasing the size did not change the quantitative description of any of the potentials by a noteworthy amount. The data are presented in Tables VIII, IX, and X, wherein we have reported the minimum absolute energy for a given J, and the relative energy of the other states relative to this minimum. In Figs. 3–6, are schematics of the $J=0$ and $J=1$ states for the experimental data and these six potentials.

To give a proper context for the observations of the tested potentials, Fig. 3 gives a schematic of the $J=0$ and

TABLE VIII. ASP-W and ASP-S eigenstates. All energies are in cm^{-1}. The J quantum number refers to the overall cluster. The numbers give the energy of the eigenstate relative to the ground state. For example, with ASP-W $J=0$, the ground state (A_1^+) is at -986.61 cm^{-1}, the lowest A_2^- state is 4.66 cm^{-1} higher in energy, and the lowest B_2^- state is 3.45 cm^{-1} above that A_2^- state or 8.11 cm^{-1} above the ground state.

ASP-W						ASP-S					
$J=0$			$J=1$			$J=0$			$J=1$		
	B_2^-	17.41									
	E^-	13.13									
121.71	A_2^-										
	B_1^+	12.48					B_1^-	1.52			
	E^+	8.70					E^-	0.15			
119.04	A_1^+					115.24	A_1^-				
	A_1^-	6.43		B_1^+	11.09		B_1^+	18.96			
	B_1^-	0.77		E^+	10.10		E^+	8.52			
113.89	E^-		78.57	A_1^+		111.17	A_1^+				
	E^-	7.35		B_2^-	11.91		E^-	7.31			
	A_2^-	1.80		E^-	8.27		A_2^-	0.91			
90.31	B_2^-		76.64	A_2^-		97.91	B_2^-				
	E^+	11.45		A_1^-	3.38		A_1^-	13.10		A_1^-	1.63
	B_1^+	6.15		E^-	1.38		E^-	0.12		E^-	0.63
89.25	A_1^+		10.78	B_1^-		97.18	B_1^-		13.82	B_1^-	
	A_2^+	17.26		B_1^+	3.38		A_2^+	14.19		B_1^+	1.63
	E^+	1.45		E^+	1.38		E^+	11.85		E^+	0.38
83.81	B_2^+		10.78	A_1^+		93.51	B_2^+		13.82	A_1^+	
	A_1^-	14.19		A_2^+	2.89		B_1^+	10.51		A_2^+	1.26
	E^-	3.64		E^+	1.00		E^+	1.21		E^+	0.38
77.24	B_1^-		9.92	B_2^+		91.82	A_1^+		11.79	B_2^+	
	A_2^+	8.28		B_2^-	2.89		A_2^+	6.81		B_2^-	1.26
	E^+	5.33		E^-	1.00		E^+	3.06		E^-	0.38
75.55	B_2^+		9.92	A_2^-		61.22	B_2^+		11.78	A_2^-	
	B_2^-	3.45		A_2^+	3.44		B_2^-	1.53		A_2^+	1.53
	E^-	1.89		E^+	1.88		E^-	0.95		E^+	0.95
4.66	A_2^-		4.74	B_2^+		10.12	A_2^-		10.12	B_2^+	
	B_1^+	3.44		A_1^-	3.44		B_1^+	1.75		A_1^-	1.75
	E^+	2.11		E^-	2.11		E^+	1.10		E^-	1.10
-986.61	A_1^+		-986.21	B_1^-		-928.36	A_1^+		-927.97	B_1^-	

TABLE IX. NEMO3 and SW eigenstates.

NEMO3						SW					
$J=0$			$J=1$			$J=0$			$J=1$		
	A_1^-	0.74					E^-	9.24			
	E^-	0.53					B_2^-	2.61			
120.45	B_1^-					91.99	A_2^-				
	E^+	7.12		A_2^+	0.33		A_2^+	21.21		A_1^-	3.69
	A_2^+	6.62		E^+	0.25		E^+	20.99		E^-	1.65
118.21	B_2^+		18.00	B_2^-		86.18	B_2^+		14.28	B_1^-	
	A_2^-	0.30		A_1^-	0.35		A_1^-	25.43		B_1^+	3.69
	E^-	0.20		E^-	0.07		E^-	4.74		E^+	1.65
112.78	B_2^-		16.99	B_1^-		80.41	B_1^-		14.29	A_1^+	
	B_1^+	0.90		B_1^+	0.35		B_1^+	34.98		A_2^+	2.74
	E^+	0.54		E^+	0.07		E^+	14.99		E^+	0.81
107.61	A_1^+		16.99	A_1^+		64.89	A_1^+		12.80	B_2^+	
	A_2^+	0.66		A_2^+	0.24		A_2^+	20.40		B_2^-	2.75
	E^+	0.45		B_2^+	0.02		E^+	6.36		E^-	0.81
49.57	B_2^+		13.43	E^+		43.43	B_2^+		12.79	A_2^-	
	B_2^-	0.33		B_2^-	0.24		B_2^-	3.00		A_2^+	2.99
	E^+	0.25		A_2^-	0.02		E^-	1.76		E^+	1.75
18.00	A_2^-		13.42	E^-		11.57	A_2^-		11.56	B_2^+	
	B_1^+	0.37		A_1^-	0.37		B_1^+	3.89		A_1^-	3.89
	E^+	0.32		E^-	0.32		E^+	2.17		E^-	2.16
−1004.08	A_1^+		−1003.68	B_1^-		−1030.49	A_1^+		−1030.07	B_1^-	

$J=1$ $(H_2O)_2$ tunneling splittings derived from experiment. It should be noted that the interchange and acceptor switching tunneling splittings cannot be measured spectroscopically due to the fact that some states in $(H_2O)_2$ have a zero spin weight and that transitions across the acceptor switching components and across the interchange are symmetry forbidden. The splittings presented here were calculated via a fit of the available RF, microwave, and far-infrared spectra to the local-IAM model of Coudert and Hougen and are presumed to represent a very good estimate of the true splittings.[44,67]

A quick inspection of the figures makes it immediately clear that none of the potentials shown here can reproduce the experimental splittings. The ASP-S surface with the Szczęśniak dispersion model,[68] is the closest of the six tested here, with an interchange splitting about 2.5 times too large and an acceptor splitting that is within 10% of the experi-

TABLE X. MCY-KW and MCY eigenstates.

MCY-KW						MCY					
$J=0$			$J=1$			$J=0$			$J=1$		
	E^+	3.28					A_1^-	18.20			
	B_1^+	0.23					B_1^-	17.93			
153.34	A_1^+					144.16	E^-				
	B_2^-	0.09		E^+	0.12		E^-	0.24		E^+	0.17
	A_2^-	0.07		A_2^+	0.04		B_1^+	0.14		A_2^+	0.04
143.49	E^-		18.81	B_2^+		141.44	A_1^+		18.74	B_2^+	
	E^-	0.10		A_1^-	0.14		E^-	0.21		E^+	4.78
	A_1^-	0.09		B_1^-	0.11		A_1^-	0.15		A_2^+	0.03
136.81	B_1^-		17.92	E^-		138.47	B_1^-		13.37	B_2^+	
	E^+	0.68		B_1^+	0.14		E^+	0.19		E^-	4.78
	B_1^+	0.09		A_1^+	0.11		B_1^+	0.07		A_1^-	0.03
135.54	A_1^+		17.92	E^+		130.96	A_1^+		13.37	B_1^-	
	E^+	0.23		A_2^+	0.16		E^+	0.31		B_1^+	5.16
	A_2^+	0.06		B_2^+	0.13		A_2^+	0.08		A_1^+	5.12
55.67	B_2^+		13.24	E^+		57.00	B_2^+		13.20	E^+	
	E^-	0.12		B_2^-	0.15		E^-	0.17		A_1^-	5.16
	B_2^-	0.04		A_2^-	0.13		B_2^-	0.04		B_1^-	5.12
18.81	A_2^-		13.24	E^-		18.74	A_2^-		13.19	E^-	
	E^+	0.17		E^-	0.17		E^+	0.22		E^-	0.22
	B_1^+	0.04		A_1^-	0.04		B_1^+	0.05		A_1^-	0.04
−1348.86	A_1^+		−1348.44	B_1^-		−1344.70	A_1^+		−1344.28	B_1^-	

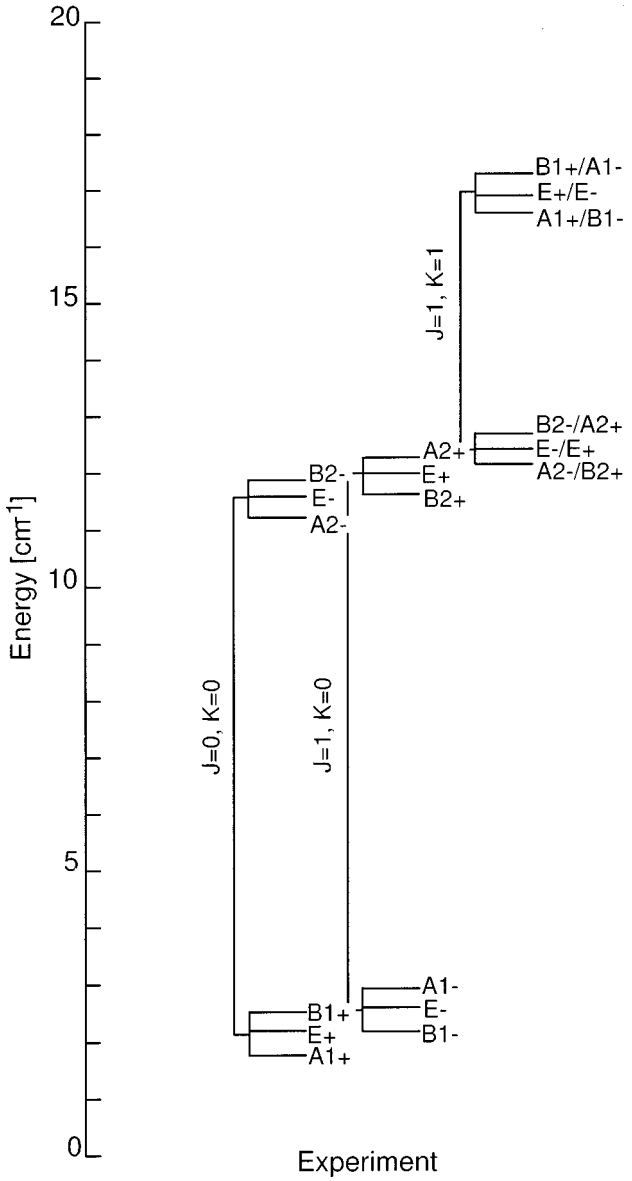

FIG. 3. Experimental energy level diagram.

mental value. The ASP-W surface, which differs from the ASP-S surface by replacing the dispersion terms with the more exhaustive multipole expansion due to Wormer *et al.*,[69,70] fairs much worse with interchange splittings 4 times too large and an acceptor splitting that is a factor of 2 too small. The SW surface, a distributed multipole potential similar to but less complicated than the ASP potentials, produces an acceptor splitting that is about 2 cm^{-1} too large, as well as interchange splittings that are 5 times larger than experiment. The NEMO, MCY, and MCY-KW surfaces all have interchange splittings that are much too small and acceptor splittings that are 2 times too large. It is interesting to note that although the latter three potentials have very dissimilar functional forms (NEMO employs distributed charges, dipoles, and polarizabilities on all the atomic sites; MCY is a simple point charge model fitted to a SCF/CI surface; MCY-KW is a reformulation of MCY with an explicit polarizable term added at the oxygens), their energy level diagrams are remarkably similar. Also calculated but not shown in this paper are the SPC,[71] polarizable SPC,[72] RWK2,[73] and TIP4P (Ref. 74) potentials which have ground state splittings nearly identical to MCY.

B. Comparison to other methods

As noted before, the findings presented in the first SWPS paper were erroneous due to a subtle error in the definition of the monomer internal axis system. The correctness of the present implementation of our code has recently been confirmed by demonstrating quantitative agreement with DVR results of van der Avoird[75] and Light[76] using the RWK2 and ASP-W potentials, repectively.

Previously, we had found that Althorpe and Clary's DVR reverse adiabatic approximation (RAA) (Ref. 50) to be less than adequate in calculating the ground state tunneling splittings and attributed the deficiency to the fact that in the RAA scheme, the radial coordinate is decoupled from the angular coordinates. This is in direct contrast to the SWPS algorithm where all coordinates are fully coupled. Reexamination of the RAA results in comparison to our present calculations, however, show that the RAA data are reasonably close to the fully coupled 6D calculations. The absolute energies of the ASP-S potential from the RAA code, for example, are within 3 cm^{-1}, and the tunneling splittings deviate on the order of 0.2 cm^{-1}. This is in quite good agreement, especially in light of the fact that in the RAA report only three radial points were sampled and the angular basis was severely truncated to $j_{\max}=8$ and $k_{\max}=4$.

C. The intermolecular vibrations

The low energy intermolecular vibrations have been investigated in several papers both with *ab initio* and empirical potentials. Reimers and Watts reported the normal-mode and anharmonic corrected frequencies for the RWK2 potential and provide a pictorial description of the six low frequency modes which are reproduced in Fig. 7.[52] They determine that the ordering of the modes, starting with the lowest energy, is ν_{12}, an A'' donor torsion of the free hydrogen, ν_8, an A' wag of the acceptor, and ν_{11}, an A'' acceptor twist.

To examine the lowest (below 150 cm^{-1}) excited intermolecular vibrations, calculated bands are presented in Table XI. For comparison, we have included the values from the work of Reimers and Watts. To assign the vibrational symmetry from the data, we note that in the absence of tunneling, the appropriate PI symmetry group is $C_s(M)$, where the allowed states A' and A''. When all tunneling motions are allowed (without the breaking of any chemical bonds), the group is then G_{16}. The correlation from $C_s(M)$ to G_{16} for the even J states is

$$\Gamma_{A'}=A_1^+\oplus E^+\oplus B_1^+\oplus A_2^-\oplus E^-\oplus B_2^-,$$

$$\Gamma_{A''}=B_1^-\oplus E^-\oplus A_1^-\oplus B_2^+\oplus E^+\oplus A_2^+.$$

To produce the appropriate correlation for the odd J states, the A' and A'' labels are exchanged. The band origins of the excited VRT states are formed by pairing the interchange triplets for a given symmetry and determining the midpoint of this pair. As an example, to find the band origin of the

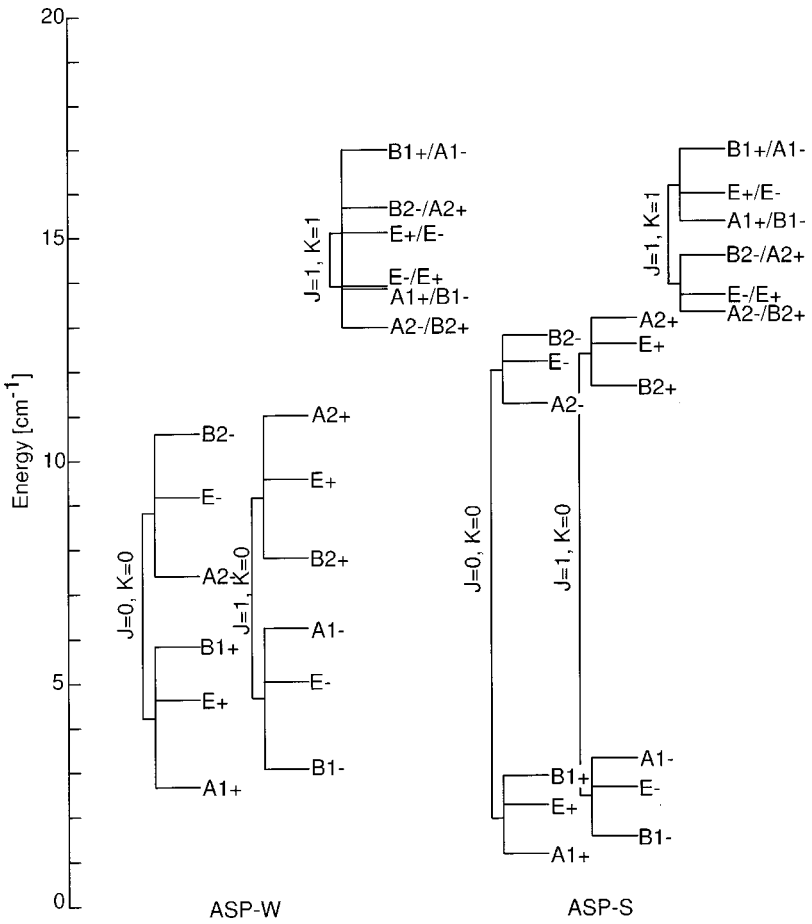

FIG. 4. Energy level diagrams for the ASP potentials.

lowest A'' for the ASP-W data, Table VIII shows that there is an $B_2^+/E^+/A_2^+$ interchange triplet at 75.55 cm^{-1}, and its companion $B_1^-/E^-/A_1^-$ interchange triplet at 77.24 cm^{-1}. The band origin of the first A'' vibration would then be 76.40 cm^{-1}. If more than one pairing was available, we chose the pair that produced the smallest acceptor tunneling splitting based upon the observation that most of the potentials overestimate the ground state value. As the eigenvectors were not computed in this work, we are not currently able to specify the nature of these vibrations.

We see that the ordering of the A' or A'' symmetry of the first three modes is the same as calculated by Reimers and Watts, however, their normal-mode frequencies are higher by as much as a factor of 2. Also, the acceptor tunneling splitting varies dramatically between potentials. This splitting in the lowest A'' band, for example, is a mere 1.9 cm^{-1} on the ASP-W surface and increases to 36 cm^{-1} with ASP-S, and is greater than 80 cm^{-1} on the MCY and MCY-KW surfaces. Similarly, the acceptor splitting in the lowest A' band varies between 0.9 cm^{-1} on ASP-W to 27.1 cm^{-1} on SW.

VI. DISCUSSION

The 6D SWPS results presented here, and corrected for the errors present in our previous treatment, demonstrate that both the RAA and DQMC methods can produce results that are qualitatively accurate. These methods can therefore be applied as a fast method of accessing the numerous water potentials that exist in the literature. To achieve quantitative accuracy, however, it is necessary to have a fully coupled 6D treatment of the Hamiltonian. With recent improvements to the SWPS code, and a reasonably sized basis set, it now feasible to use the SWPS code as the primary method for characterizing the VRT dynamics on 6D potentials. As an example of the computational time required, with a basis of $j_{max}=9$ and 6 radial points, the SWPS code can fully converge the lowest three eigenstates of all ten symmetries for $J=0$ and $J=1$ in less than 23 h on an IBM RS/6000 590.

An important conclusion presented before, viz., that none of the potentials examined thus far exhibit an acceptable agreement with experiment, still holds. Most of the potentials that we have explored greatly overestimate the acceptor tunneling splitting and underestimate the donor–acceptor interchange splitting in the ground state. The more rigorous ASP and SW potentials fare best in this respect, but still fall far short of achieving spectroscopic accuracy. In particular, the two ASP potentials, which differ only in their treatment of the dispersion forces, demonstrate that modern *ab initio* methods are still limited in their ability to rigorously describe the water dimer pair potential. It is notable that none of the potentials have a dissociation energy (D_0) that agrees with the best available experimental measurement of 1250 cm^{-1} (3.59 ± 0.5 kcal/mol).[77] D_0's of the MCY and MCY-KW surfaces are approximately 0.3 kcal/mol too strong where as the others are too weakly bound by about 0.7–0.9 kcal/mol. However, we note that the present calcu-

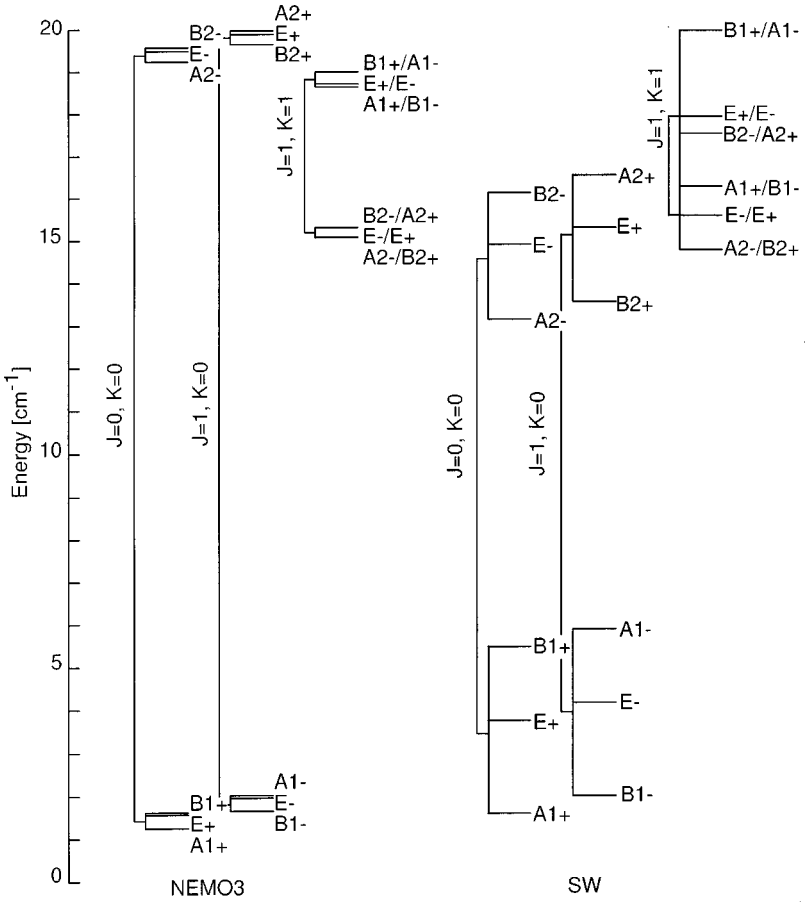

FIG. 5. Energy level diagrams for the NEMO3 and SW potentials.

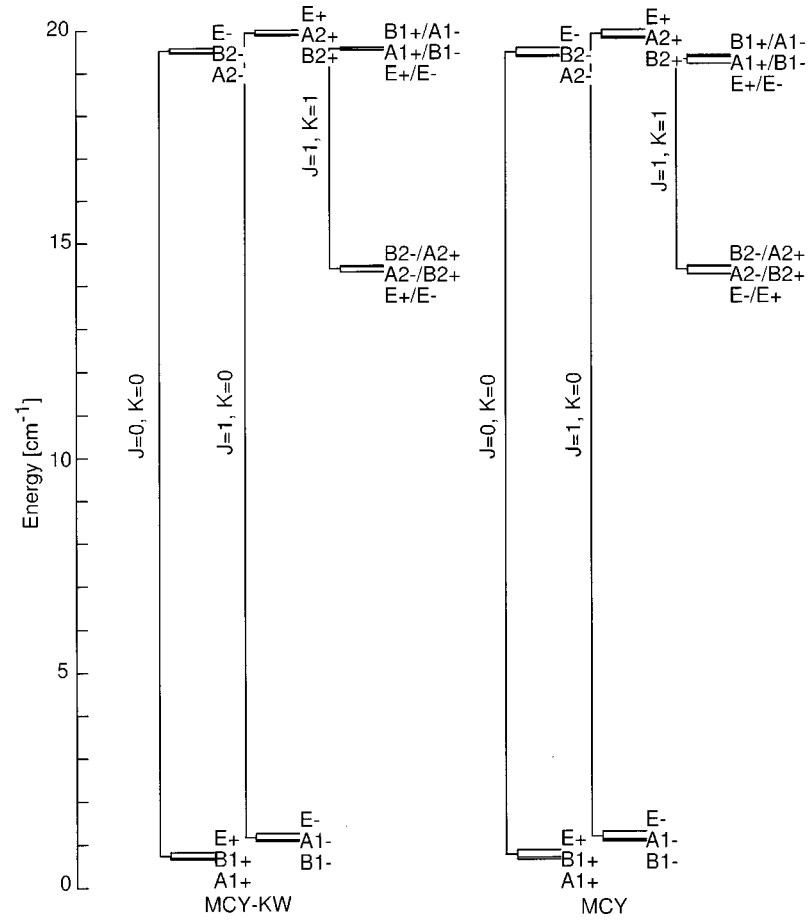

FIG. 6. Energy level diagrams for the MCY-KW and MCY potentials.

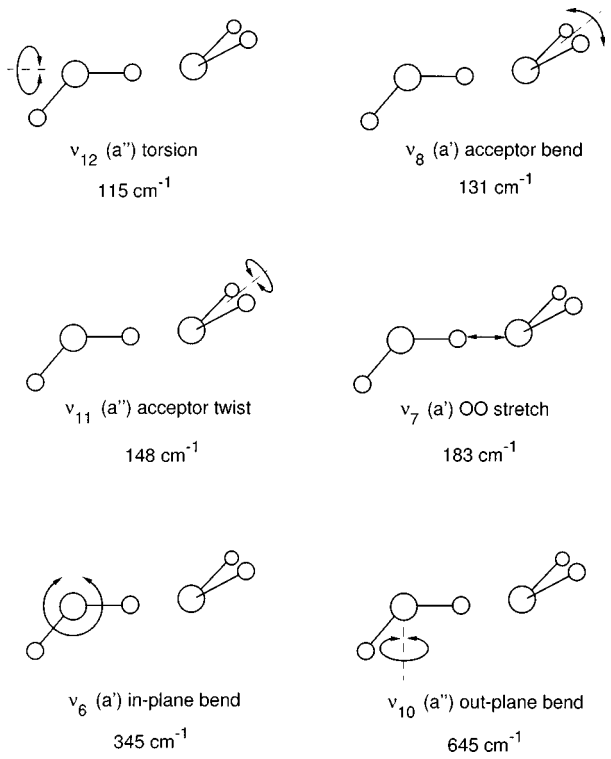

FIG. 7. Normal modes with harmonic frequencies for the water dimer $(H_2O)_2$ from Reimers and Watts (Ref. 52).

TABLE XI. The three lowest energy intermolecular modes of the water dimer for the six potentials investigated. The method for assigning the symmetry is explained in the text.

	Vib. symmetry	Band origin	Acceptor splitting[c]
	A''	219	⋯
Reimers and Watts[a]	A'	169	⋯
	A''	115	⋯
	A''	98.85	30.25
ASP(W)	A'	89.78	0.88
	A''	76.40	1.92
	A''	102.34	17.66
ASP(S)	A'	94.87	6.09
	A''	79.20	35.96
	A''	123.65	10.88
NEMO	A'	110.20	5.17
	A''	85.01	70.88
	A''	104.06	18.94
SW	A'	78.44	27.10
	A''	61.88	36.98
	A''	154.78	9.22
MCY-KW	A'	139.52	7.95
	A''	96.24	81.14
	⋯	⋯	⋯
MCY[b]	⋯	⋯	⋯
	A''	97.74	81.47

[a]Harmonic frequencies for the RWK2 potential (Ref. 52). Tunneling splittings were not reported in this work.
[b]The second and third band origin could not be determined because the required interchange pairs did not appear below 150 cm^{-1}.
[c]Acceptor tunneling splittings are determined by the difference of the lowest energy eigenstates for each interchange triplet.

lations employ rigid monomer, and relaxation of the constraint will affect this conclusion. Such effects are currently under study.

A more striking manifestation of the deficiencies of these potentials is the disparity in the description of excited vibrational states. As shown in Table XI, the apparent ordering of the three lowest excited states of all the tested potentials (except MCY) agree with the harmonic frequencies calculated from RWK2 as well as with the results from a number of other potentials and *ab initio* calculations.[54,78] There are, however, dramatic variations in the calculated tunneling splittings spanning several orders of magnitude. It is not clear why there is little qualitative agreement between the investigated potentials but a clue may be found in the recent work of Millot *et al.*[78] where they performed an extensive search for stationary points on 14 water potentials. In that report, the authors determined a number of first order saddle points on the various potentials (the first order saddle points correspond to transition state structures of the presumed hydrogen bond rearrangement tunneling pathways) and compared them to supermolecule ab initio calculations of Smith *et al.* (SSPSR) (Ref. 55) and Wales.[56]

This study shows, quite dramatically, that none of the 14 potentials are able to qualitatively reproduce the stationary point structures and energetics found by SSPSR or Wales. In fact, the set of ASP surfaces [ASP-W (Ref. 61), ASP-W2 (Ref. 78), and ASP-W4 (Ref. 78), which we collectively refer to as ASP] all show more transition state structures than SSPSR suggesting a greater number of rearrangement pathways than the three detailed in Sec. II. This feature of the ASP surfaces is particularly striking in light of the complexity of the ASP functional form (distributed multipole analysis[79]) and the level of *ab initio* theory used to determine its parameters (MP2 or multireference CI).

At first glance, one may take the SSPSR or Wales results as being a more accurate representation of the water dimer IPS. However, it has been shown in that work[55] that the details of the surface are sensitive to the level of theory and size of the basis set. Additionally, the basis set superposition error (BSSE) has a large orientation dependence. BSSE can be estimated by the counterpoise method (CP) but presently cannot be included in a gradient search for stationary points thus questioning the extent to which one should use the SSPSR results in characterizing the hydrogen bond rearrangement dynamics of the water dimer.

In contrast, ASP is determined via a perturbative *ab initio* method, IMPT,[79] which eliminates the BSSE problem. In the case where the H_2O monomer properties can be described completely and accurately (i.e., charge distribution, polarizability, and dispersion), ASP should be able to describe the true water dimer IPS with unprecedented accuracy. This limit is not realized, however, since some properties, viz., dispersion and associated damping functions, are difficult to measure or calculate. In addition, since the monomer properties are fitted to spherical harmonic expansions of finite order, the resultant surface may have defects (e.g., dimples on a smooth surface) that can lead to the discovery

of false stationary points and give a misleading picture of the hydrogen bond rearrangement dynamics.

Most water potentials and *ab initio* theory agree on the ground state equilibrium structure of the dimer but the range of the estimated equilibrium binding energy (D_e) is disturbingly wide (ca. -4.3 to -5.9 kcal/mol). From examination of the article of Millot *et al.*[78] and our calculated VRT states, it is evident that most of the details of the dimer IPS are still in question. A natural path to solving this problem is to determine a new potential by least squares inversion of VRT data.

ACKNOWLEDGMENTS

C. Millot, A. J. Stone, G. Karlström, and R. Wheatley, are gratefully acknowledged for providing the source code of their respective potentials. This work was supported by the Experimental Physical Chemistry Program of the National Science Foundation and the France–Berkeley Cooperative Grant Program. R.J.S. is a UC-Berkeley Miller Research Professor, 1997–1998.

[1] N. Pugliano and R. J. Saykally, J. Chem. Phys. **96**, 1832 (1992).
[2] N. Pugliano, J. D. Cruzan, J. G. Loeser, and R. J. Saykally, J. Chem. Phys. **98**, 6600 (1993).
[3] K. Liu, J. G. Loeser, M. J. Elrod, B. C. Host, J. A. Rzepiela, and R. J. Saykally, J. Am. Chem. Soc. **116**, 3507 (1994).
[4] J. D. Cruzan, M. G. Brown, K. Liu, L. B. Braly, and R. J. Saykally, J. Chem. Phys. **105**, 6634 (1996).
[5] K. Liu, J. D. Cruzan, and R. J. Saykally, Science **271**, 929 (1996), and references therein.
[6] K. Liu, J. K. Gregory, M. G. Brown, C. Carter, and R. J. Saykally, Nature (London) **381**, 501 (1996).
[7] K. Liu, R. S. Fellers, M. R. Viant, R. P. McLaughlin, M. G. Brown, and R. J. Saykally, Rev. Sci. Instrum. **67**, 410 (1996).
[8] K. Liu, M. G. Brown, J. D. Cruzan, and R. J. Saykally, Science **271**, 62 (1996).
[9] K. Liu, M. G. Brown, M. R. Viant, J. D. Cruzan, and R. J. Saykally, Mol. Phys. **89**, 1373 (1996).
[10] K. Liu, M. G. Brown, and R. J. Saykally, J. Phys. Chem. A **101**, 8995 (1997).
[11] J. K. Gregory, D. C. Clary, K. Liu, M. G. Brown, and R. J. Saykally, Science **275**, 814 (1997).
[12] J. B. Paul, R. A. Provencal, and R. J. Saykally, J. Phys. Chem. A **102**, 3279 (1998).
[13] M. J. Elrod and R. J. Saykally, J. Chem. Phys. **103**, 933 (1995).
[14] E. H. T. Olthof, A. van der Avoird, and P. E. S. Wormer, J. Mol. Struct. **307**, 201 (1994).
[15] E. H. T. Olthof, A. van der Avoird, and P. E. S. Wormer, J. Chem. Phys. **101**, 8430 (1994).
[16] W. Yang and A. C. Peet, Chem. Phys. Lett. **153**, 98 (1988).
[17] R. C. Cohen and R. J. Saykally, J. Phys. Chem. **94**, 7991 (1990).
[18] R. C. Cohen and R. J. Saykally, J. Chem. Phys. **98**, 6007 (1993).
[19] C. A. Schmuttenmaer, R. C. Cohen, and R. J. Saykally, J. Chem. Phys. **101**, 146 (1994).
[20] J. C. Light, I. P. Hamilton, and J. V. Lill, J. Chem. Phys. **82**, 1400 (1985).
[21] C. Lanczos, J. Res. Natl. Bur. Stand. **45**, 225 (1950).
[22] D. C. Sorenson, SIAM J. Matrix Anal. Appl. **13**, 357 (1992).
[23] P. P. Korambath, X. T. Wu, and E. F. Hayes, J. Phys. Chem. **100**, 6116 (1996).
[24] Y. Qiu and Z. Bačić, J. Chem. Phys. **106**, 2158 (1997).
[25] Y. Qiu, J. H. Zhang, and Z. Bačić, J. Chem. Phys. **108**, 4804 (1998).
[26] M. D. Feit, J. D. Fleck, and A. Steiger, J. Comput. Phys. **47**, 412 (1982).
[27] M. D. Feit and J. D. Fleck, J. Chem. Phys. **78**, 301 (1983).
[28] D. Kosloff and R. Kosloff, J. Comput. Phys. **52**, 35 (1983).
[29] R. Kosloff and D. Kosloff, J. Chem. Phys. **79**, 1823 (1983).
[30] R. A. Friesner, J. A. Bentley, M. Menou, and C. Leforestier, J. Chem. Phys. **99**, 324 (1993).
[31] C. Leforestier, J. Chem. Phys. **101**, 7357 (1994).
[32] C. Leforestier, L. B. Braly, K. Liu, M. J. Elrod, and R. J. Saykally, J. Chem. Phys. **106**, 8527 (1997).
[33] R. G. A. Bone, D. Kosloff, T. W. Rowlands, N. C. Handy, and A. J. Stone, Mol. Phys. **72**, 33 (1991).
[34] T. R. Dyke, J. Chem. Phys. **66**, 492 (1977).
[35] T. R. Dyke, K. M. Mack, and J. S. Muenter, J. Chem. Phys. **66**, 498 (1977).
[36] J. A. Odutola and T. R. Dyke, J. Chem. Phys. **72**, 5062 (1980).
[37] L. H. Coudert, F. J. Lovas, R. D. Suenram, and J. T. Hougen, J. Chem. Phys. **87**, 6290 (1987).
[38] J. A. Odutola, T. A. Hu, D. Prinslow, S. E. O'Dell, and T. R. Dyke, J. Chem. Phys. **88**, 5352 (1988).
[39] G. T. Fraser, R. D. Suenram, and L. H. Coudert, J. Chem. Phys. **90**, 6077 (1989).
[40] T. A. Hu and T. R. Dyke, J. Chem. Phys. **91**, 7348 (1989).
[41] R. D. Suenram, G. T. Fraser, and F. J. Lovas, J. Mol. Spectrosc. **138**, 440 (1989).
[42] E. Zwart, J. J. T. Meulen, and W. L. Meerts, Chem. Phys. Lett. **166**, 500 (1990).
[43] E. Zwart, J. J. T. Meulen, and W. L. Meerts, Chem. Phys. Lett. **173**, 115 (1990).
[44] E. Zwart, J. J. T. Meulen, and W. L. Meerts, J. Mol. Spectrosc. **147**, 27 (1991).
[45] E. N. Karyakin, G. T. Fraser, and R. D. Suenram, Mol. Phys. **78**, 1179 (1993).
[46] Z. S. Huang and R. E. Miller, J. Chem. Phys. **91**, 6613 (1989).
[47] L. B. Braly, J. D. Cruzan, K. Liu, and R. J. Saykally (in preparation).
[48] M. Lewerenz and R. O. Watts, J. Chem. Phys. (in press).
[49] J. K. Gregory and D. C. Clary, J. Chem. Phys. **102**, 7817 (1995).
[50] S. C. Althorpe and D. C. Clary, J. Chem. Phys. **101**, 3603 (1994).
[51] S. Scheiner, Annu. Rev. Phys. Chem. **45**, 23 (1994).
[52] J. R. Reimers and R. O. Watts, Chem. Phys. **85**, 83 (1984).
[53] M. J. Frisch, J. E. D. Bene, J. S. Binkley, and H. F. Schaefer, J. Chem. Phys. **84**, 2279 (1986).
[54] P. O. Åstrand, G. Karlström, A. Engdahl, and B. Nelander, J. Chem. Phys. **102**, 3534 (1995).
[55] B. J. Smith, D. J. Swanton, J. A. Pople, H. F. Schaefer, and L. Radom, J. Chem. Phys. **92**, 1240 (1990).
[56] D. J. Wales, in *Theory of Atomic and Molecular Clusters 2*, edited by J. Jellick (Springer, Heidleberg, 1998), http://brian.ch.cam.ac.uk/publications.html.
[57] G. Brocks, A. van der Avoird, B. T. Sutcliffe, and J. Tennyson, Mol. Phys. **50**, 1025 (1983).
[58] J. Echave and D. C. Clary, Chem. Phys. Lett. **190**, 225 (1992).
[59] D. O. Harris, G. G. Engerholm, and W. D. Gwinn, J. Chem. Phys. **43**, 1515 (1965).
[60] B. W. Shore, J. Chem. Phys. **59**, 6450 (1973).
[61] C. Millot and A. J. Stone, Mol. Phys. **77**, 439 (1992).
[62] The approximate relationship between the number of DVR points and the monomer quantum numbers j, k, and ω are $j \mapsto N_\theta = j+3$, $k \mapsto N_\chi = (2k+1)+2$, and $\omega \mapsto N_\phi = (2\omega+1)+2$. If $j_{\max} = k_{\max} = \omega_{\max}$, then the number of DVR points, floating point operations, will scale as $O(N_\theta^a \times N_\theta^b \times N_\chi^b \times N_\chi^b \times N_\phi)$ or $O(j_{\max}^5)$.
[63] O. Matsuoka, E. Clementi, and M. Yoshimine, J. Chem. Phys. **64**, 1351 (1976).
[64] P. O. Åstrand, P. Linse, and G. Karström, Chem. Phys. **191**, 195 (1995).
[65] S. Kuwajima and A. Warshel, J. Phys. Chem. **94**, 460 (1990).
[66] R. J. Wheatley, Mol. Phys. **87**, 1083 (1996).
[67] L. H. Coudert and J. T. Hougen, J. Mol. Spectrosc. **139**, 259 (1990).
[68] M. M. Szczęśniak, R. J. Brenstein, S. M. Cybulski, and S. Scheiner, J. Phys. Chem. **94**, 1781 (1990).
[69] W. Rijks and P. E. S. Wormer, J. Chem. Phys. **90**, 6507 (1989).
[70] P. E. S. Wormer and H. Hettema, J. Chem. Phys. **97**, 5592 (1992).
[71] H. J. C. Berendsen, J. P. M. Postma, W. F. van Gunsteren, and J. Hermans, in *Intermolecular Forces*, edited by B. Pullman (Reidel, Dordrecht, 1981).
[72] D. N. Bernardo, Y. Ding, K. Krogh-Jespersen, and R. M. Levy, J. Phys. Chem. **98**, 4180 (1994).
[73] J. R. Reimers, R. O. Watts, and M. L. Klein, Chem. Phys. **64**, 95 (1982), and references therein.
[74] W. L. Jorgensen, J. Chem. Phys. **77**, 4156 (1982).
[75] A. van der Avoird (private communication).
[76] J. C. Light (private communication).

[77] L. A. Curtiss, D. J. Frurip, and M. Blander, J. Chem. Phys. **71**, 2703 (1979).
[78] C. Millot, J. C. Soetens, M. T. C. Martins-Costa, M. P. Hodges, and A. J. Stone, J. Phys. Chem. A **102**, 754 (1998).
[79] A. J. Stone, *The Theory of Intermolecular Forces, The International Series of Monographs on Chemistry* (Clarendon, Oxford, 1996).
[80] J. W. I. van Bladel, A. van der Avoird, and P. E. S. Wormer, J. Phys. Chem. **95**, 5414 (1991).